Characterization of protein resistant, grafted methacrylate polymer layers bearing oligo(ethylene glycol) and phosphorylcholine side chains by neutron reflectometry

Wei Feng
Department of Chemical Engineering, McMaster University, Hamilton, Ontario L8S 4L7, Canada and School of Biomedical Engineering, McMaster University, Hamilton, Ontario L8S 4L7, Canada

Mu-Ping Nieh
Canadian Neutron Beam Centre, National Research Council, Chalk River, Ontario K0J 1J0, Canada

Shiping Zhu
Department of Chemical Engineering, McMaster University, Hamilton, Ontario L8S 4L7, Canada and School of Biomedical Engineering, McMaster University, Hamilton, Ontario L8S 4L7, Canada

Thad A. Harroun
Department of Physics, Brock University, St. Catharines, Ontario L2S 3A1, Canada

John Katsaras
Canadian Neutron Beam Centre, National Research Council, Chalk River, Ontario K0J 1J0, Canada; Department of Physics, Brock University, St. Catharines, Ontario L2S 3A1, Canada; Guelph-Waterloo Physics Institute, University of Guelph, Guelph, Ontario N1G 2W1, Canada; and the Biophysics Interdepartmental Group, University of Guelph, Guelph, Ontario N1G 2W1, Canada

John L. Brash[a)]
Department of Chemical Engineering, McMaster University, Hamilton, Ontario L8S 4L7, Canada and School of Biomedical Engineering, McMaster University, Hamilton, Ontario L8S 4L7, Canada

(Received 19 December 2006; accepted 31 January 2007; published 29 March 2007)

Neutron reflectometry was used to investigate the structures of end-tethered protein resistant polymer layers based on poly(oligo(ethylene glycol) methyl ether methacrylate) [poly(OEGMA)] and poly(2-methacryloyloxyethyl phosphorylcholine) [poly(MPC)]. Layers having different graft densities were studied in both the dry and wet states. A stretched parabolic model was used to fit the neutron data, resulting in a one-dimensional scattering length density profile of the polymer volume fraction normal to the film. Measured in D_2O, the cutoff thicknesses of OEGMA and MPC layers at high graft density (0.39 chains/nm^2 for OEGMA and 0.30 chains/nm^2 for MPC) and a chain length of 200 repeat units were 450 and 470 Å, respectively, close to their contour length of 500 Å, suggesting that the grafts become highly hydrated when exposed to water. It was also found that at similar graft density and chain length, the volume fraction profiles of poly(OEGMA) and poly(MPC) layers are similar, in line with the authors' previous results showing that these surfaces have similar protein resistance [W. Feng *et al.*, BioInterphases **1**, 50 (2006)]. The possible correlation of protein resistance to water content as indicated by the average number of water molecules per ethylene oxide ($N_{w,EO}$) or phosphorylcholine ($N_{w,PC}$) moiety was investigated. $N_{w,EO}$ and $N_{w,PC}$, estimated from the volume fraction data, increased with decreasing graft density, and when compared to the reported number of water molecules in the hydration layers of EO and PC residues, led to the conclusion that water content slightly greater than the water of hydration resulted in protein resistant surfaces, whereas water content either less than or greatly in excess of the water of hydration resulted in layers of reduced protein resistance. © *2007 American Vacuum Society.* [DOI: 10.1116/1.2711705]

I. INTRODUCTION

The development of surfaces which prevent nonspecific protein adsorption is important for many biomedical and biotechnology applications including biomaterials, biochips, and biosensors.[1–5] Uncontrolled protein adsorption from biological fluids results in the fouling of biointerfaces. In tissue contacting applications, nonspecific protein adsorption may promote the adhesion of macrophages and other cells, leading to inflammatory and foreign body responses. For devices in contact with blood, even small quantities of adsorbed protein may initiate coagulation as well as platelet adhesion and activation, leading ultimately to thrombus formation. Preventing nonspecific protein adsorption is thus of critical importance in the design of biomedical and bioanalytical devices. For this purpose, the modification of biointerfaces

[a)]Author to whom correspondence should be addressed; electronic mail: brashjl@mcmaster.ca

with poly(ethylene oxide) (PEO) (Refs. 6 and 7) or with polymers based on phosphorylcholine[8–10] (PC) has been found to be effective.

The mechanisms of PEO- and PC-mediated protein resistance are presently not clear, but it is recognized that polymer chain length, graft density, and the structural arrangement of water molecules associated with the PEO- and PC-containing layers are important factors in determining the interactions of the surface with proteins.[7,11–14] In general, protein adsorption decreases with increasing polymer chain length and graft density. More recently, an optimal graft density giving minimal protein adsorption was found for tethered PEO layers. Densities above as well as below this optimal value gave surfaces of lower protein resistance.[15–17] Moreover, neutron reflectometry (NR) experiments have suggested that the water volume fraction in tethered PEO chains is critical in determining protein interactions.[18] Monte Carlo simulations[19] and *ab initio* calculations[20] both predicted that, for the most part, the ether oxygens in the outermost layer, and even those ether oxygens adjacent to the outermost layer in the tethered PEO chains with helical conformation, are involved in hydrogen bonds with water molecules. These results agree well with the data obtained by vibrational sum-frequency generation spectroscopy.[21] Ishihara and coworkers found that there is a larger fraction of "free" water in PC-containing copolymers than in other water-soluble (co-)polymers, such as poly(2-hydroxyethyl methacrylate) and poly(*N*-vinyl pyrrolidone-*co*-*n*-butyl methacrylate). The highly hydrated layer associated with the PC headgroups is believed to result in decreased protein adsorption and improved biocompatibility.[22] Recently, using polarized Raman and attenuated total reflection infrared spectroscopies, Kitano *et al.*[23,24] investigated the hydrogen-bond network structure of the water molecules in the vicinity of various water-soluble polymers and calculated the number of hydrogen bonds per monomer unit in the water which are "collapsed" ($N_{\text{collapsed}}$) by the presence of polymer. They found that in the case of PEO- and PC-containing polymers, $N_{\text{collapsed}}$ is practically zero and much smaller than for other polymers, suggesting that PEO- and PC-containing polymers do not significantly disturb the hydrogen bonding between water molecules. Apparently, water plays a crucial role in modulating the interactions between PEO- and PC-enriched surfaces and proteins.[23,24]

Comparison of PEO- and PC-based systems with respect to their effectiveness in preventing protein adsorption has been reported previously.[25] Silicon (Si) surfaces grafted with oligo(ethylene glycol) methyl ether methacrylate (OEGMA) and 2-methacryloyloxyethyl phosphorylcholine (MPC), which contain, respectively, PEO and PC sidechains of comparable size, were chosen as the basis for this comparison. Using single and binary protein solutions, no significant difference was found between the MPC and OEGMA surfaces for a given chain length and graft density.[25]

Neutron reflectometry is a nondestructive and powerful tool capable of elucidating the structural details of tethered polymer layers and has been used widely to investigate polymer/solvent interactions under a variety of conditions.[26–28] For example, Yim *et al.*[29] applied NR to study the temperature-dependent conformational changes of poly(N-isopropylacrylamide) (PNIPAM) chains grafted on Si wafers. They found that at an intermediate graft density, the long chains of PNIPAM undergo maximum conformational change between 25 and 30 °C.

Using NR, the objective of the present work was to determine the thickness and volume fraction profiles of poly(OEGMA) and poly(MPC) thin films grafted on Si wafers in both the dry and wet states. Additional motivation was the capability of NR to provide information on the average number of water molecules per EO or PC residue for possible correlation to protein adsorption behavior.

II. EXPERIMENT

A. Materials

9-Decen-1-ol (97%), 2-bromo-2-methylpropionyl bromide (98%), trichlorosilane (99%), hydrogen hexachloroplatinate (IV) hydrate (H_2PtCl_6, 99.9%), 2,2′-bipyridine (bpy, 99%), Cu(I)Br (99.99%), methoxy poly(ethylene glycol) ($M_n \sim 350$ g/mol), ethyl 2-bromoisobutyrate (EBiB, 98%), dodecyltrichlorosilane (99%), and OEGMA ($M_n \sim 300$; PEO sidechains of $n=4.5$) were purchased from Aldrich (Oakville, ON). OEGMA was distilled over CaH_2 under vacuum and stored at −15 °C. Toluene and methanol [high-performance liquid chromatography (HPLC) grade] were obtained from Caledon Laboratories Ltd. (Georgetown, ON). Toluene was gently stirred over CaH_2 for 24 h and then distilled twice prior to use. Si wafers (4 in. diameter, 6 mm thickness) were obtained from Wafer World Inc. (West Palm Beach, FL). MPC was kindly provided by Ishihara (School of Engineering, University of Tokyo, Japan) and used without further purification. All other reagents were purchased commercially and used as received.

B. Preparation of initiator-functionalized silicon wafers

The pretreatment of Si wafers followed previously described procedures.[30] To graft polymer chains directly to silicon oxide, an organosilane containing 2-bromo isobutyrate was used as the surface-attachable atom transfer radical polymerization (ATRP) initiator. The synthetic procedure for the initiator 10-(2-bromo-2-methyl) propionyloxy decyltrichlorosilane (PDTS), is described in detail elsewhere.[31,32] The freshly cleaned wafers were placed in a 2.5 mM dry toluene solution containing the initiator PDTS or a mixture of PDTS and the diluting agent dodecyltrichlorosilane (DTS) for 18 h without stirring at room temperature. The Si wafers were removed from the solution, subjected to ultrasonication for 30 min in dry toluene, rinsed sequentially with toluene and methanol, and then dried with nitrogen gas. Two mole fractions of PDTS, i.e., 2.5% and 100%, were selected to produce monolayers containing low and high amounts of the initiator, resulting in low and high polymer graft densities, respectively.

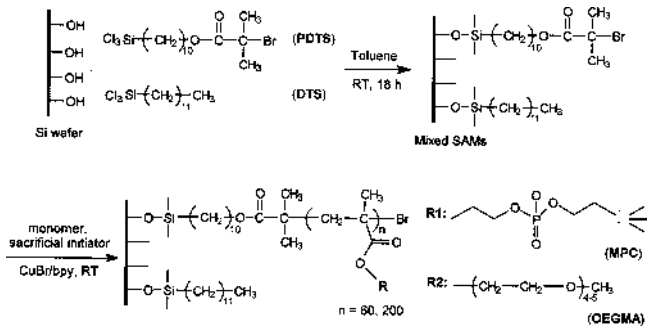

SCHEME 1. Formation of poly(OEGMA)- and poly(MPC)-grafted Si wafers with different graft densities and chain lengths using surface initiated ATRP.

C. Grafting of poly(MPC) and poly(OEGMA) from silicon

ATRP grafting of MPC and OEGMA from initiator-functionalized wafers was carried out in a glovebox purged with nitrogen following previously described procedures.[33,34] For both OEGMA and MPC grafting, Cu(I)Br/bpy was used as the catalyst and methanol as the solvent. A sacrificial initiator was added to the mixture for the following reasons: (1) to provide enough deactivator [Cu(II)Br] through the redox reaction between Cu(I)Br and the sacrificial initiator, which in turn better controls the ATRP grafting of polymers from the Si; and (2) to control the polymer chain length under the assumption that the chains grown from the Si surface and in solution have similar molecular weights. EBiB was used as sacrificial initiator for OEGMA grafting. Oligomeric methoxy polyethylene glycol 2-bromoisobutyrate, which was synthesized by the esterification of 2-bromo-2-methylpropionyl bromide with methoxy poly(ethylene glycol),[35] was used as sacrificial initiator for MPC grafting. Two different monomer/sacrificial initiator ratios (60/1 and 200/1) were used to prepare polymer-grafted Si wafers with different chain lengths. The two-step surface-initiated ATRP grafting process is shown in Scheme1. In the following sections, the polymer films are described by the first letter of the monomer (O or M), the graft density, and the chain length, e.g., O-39-200 refers to the poly(OEGMA) film with graft density of 0.39 chains/nm^2, and chain length 200.

D. Characterization of grafted polymer layers

The thicknesses of the initiator monolayers and polymer layers on the silicon substrate were obtained using an ellipsometer (Exacta 2000 ellipsometer, Waterloo Digital Electronics, Waterloo, ON) equipped with a He–Ne laser (632.8 nm). An incident angle of 70° was used for all measurements. A refractive index of 1.5 was used for the initiator and polymer layers. All measurements were conducted in air at room temperature. Graft densities were estimated using the following equation:

$$\sigma = \frac{h\rho N_A}{M_n}, \tag{1}$$

where σ is the graft density (chains/nm^2), h is the layer thickness (nm), ρ is the mass density of the grafted polymer layer [values of 1.30 and 1.15 g/cm^3, respectively, were used for poly(MPC) (Ref. 36) and poly(OEGMA) (Ref. 25)], N_A is Avogadro's number, and M_n is the number-averaged molecular weight (MW) of the grafted polymer, assumed to be the same as the polymer produced in solution using sacrificial initiators. (It should be pointed out that several studies in which both surface and solution polymerized samples were measured independently have shown their MWs to be similar.[31,37]) The MWs of poly(OEGMA) and poly(MPC) produced by the sacrificial initiator in solution were determined by gel permeation chromatography (Waters Ultrahydrogel™, 7.8×300 mm column) using a 0.2M $NaNO_3$ and 0.1% NaN_3 aqueous solution as the mobile phase. Narrow PEO samples with MW ranging from 970 to 119 000 g/mol were used as standards to generate a calibration curve. The monomer conversion in solution was determined from proton NMR spectra of the reactor contents (Brucker AC-P200 spectrometer, D_2O solvent). The characteristics of the samples used for neutron reflectometry measurements are given in Table I.

E. Neutron reflectometry experiments

NR measurements were performed using the C5 reflectometer located at the National Research Universal Reactor (Chalk River, ON). The neutron wavelength (λ) was 2.37 Å and the collimation slits were varied during the scan to en-

TABLE I. Ellipsometric and GPC characterization of surfaces used for NR measurements.

Sample	Monomer	Chain length[a]	M_n (g/mol)	M_w/M_n	Monomer conversion (%)	Ellipsometric thickness (Å)[b]	Graft density (chains/nm^2)[c]
O-39-200	OEGMA	200	49 900	1.34	96.9	281.4±2.0	0.390±0.003
O-39-60	OEGMA	60	15 500	1.27	98.9	87.7±4.6	0.390±0.021
M-30-200	MPC	200	48 400	1.25	98.5	185.5±1.5	0.300±0.002
O-07-200	OEGMA	200	49 700	1.33	97.0	51.9±3.1	0.070±0.004
M-10-200	MPC	200	48 000	1.24	98.5	63.8±2.4	0.100±0.004

[a]Molar ratio of monomer to sacrificial initiator.
[b]Average±SD based on six measurements.
[c]Calculated from Eq. (1) using ellipsometric thickness.

TABLE II. Scattering length densities (ρ) of the initiator layers and grafts employed for the calculation of NR curves.

Species	M (g/mol)	Σb_i (10^{-5} Å)	d (g/cm^3)	SLD (ρ) (10^{-6} Å^{-2})
$-C_{10}H_{20}OC(O)C(CH_3)_2-$ (PDTS)	226	7.44	1.00	0.22
$-C_{12}H_{25}$ (DTS)	169	−13.75	1.00	−0.49
Mixed monolayer (2.5% PDTS+97.5% DTS)				−0.47
$-CH_2C(CH_3)C(O)OC_2H_4PO_4^-C_2H_4N^+(CH_3)_3$ (MPC)	295	40.16	1.30[a]	1.06
$-CH_2C(CH_3)C(O)O(C_2H_4O)_{4.5}CH_3$ (OEGMA)	300	33.55	1.15[a]	0.78
D_2O	20	19.15	1.10	6.34
H_2O	18	−1.68	1.00	−0.56
Null-SLD water (8.1% D_2O+91.9% H_2O)				0.00
Si wafer				2.07
SiO_2				3.48
Air				0.00

[a]Adapted from the mass density of the polymer.

sure that the entire sample was "bathed" in neutrons as its footprint varied. Specular reflection was measured and plotted against neutron momentum transfer Q_z:

$$Q_z = (4\pi \sin \theta)/\lambda, \tag{2}$$

where θ is the angle made by incident neutrons with the sample. The range of Q_z was from 0.006 to 0.2 Å^{-1}. Measurements were performed over three Q_z regions, namely, 0.2–0.1, 0.1–0.04, and 0.04–0.006 Å^{-1}. The data were normalized using the incident beam intensity to account for variations due to slit widths and were corrected for background by setting θ to 0.5° off specular reflection.

Reflectometry experiments were carried out using samples in both the dry and wet states. Prior to measurement in the dry state, samples were cleaned with methanol (HPLC grade) and dried over nitrogen to remove any water bound to the polymer grafts. Samples were then immediately placed in the sample cell taking care to keep the layers dry. For NR measurements in the wet state, both pure D_2O and a H_2O/D_2O mixture containing 8.1% D_2O by volume to give a solvent of null scattering length density ("null-SLD water") were employed. Following the measurement in D_2O, the sample cell was flushed *in situ* with methanol (HPLC) and dried in a nitrogen stream for 1 h. Null-SLD water was then injected into the cell.

The NR sample cells used were described in detail elsewhere.[38] For dry samples, the path of the incident neutron beam was from air→sample→SiO_2→Si, while in the wet condition, the incident neutron path was from the backside of the sample, i.e., Si→SiO_2→sample→D_2O (or null-SLD water). This arrangement ensures total reflection from Si in both cases. PARRATT 32 (BENSC, Berlin) software was employed to fit the reflectivity data. In the dry state, a three-layer model was used, while a two-layer+parabolic decay model was used to fit the data in the wet state. The parabolic function can be written as[39]

$$\Phi_{\text{poly}}(z) = \Phi_{0,\text{poly}}\left(1 - \left(\frac{z}{h}\right)^2\right)^{\alpha}, \tag{3}$$

where $\Phi_{\text{poly}}(z)$ is the polymer volume fraction at a distance z from the initiator layer, $\Phi_{0,\text{poly}}$ is the polymer volume fraction at distance 0 (interface between the polymer and initiator layers), h is the cutoff thickness of the polymer layer in solvent, and α is a fitting parameter. The fitted parameters were allowed to vary so as to minimize the least-squares (χ^2) error function.

From the analysis one can determine the layer thickness (d), the surface roughness (σ), the one-dimensional SLD (ρ) as a function of z, and the volume fraction of the polymer chains (Φ_{poly}) within the layers and at the interfaces. SLDs of the ATRP surface initiator PDTS, diluting agent DTS, and grafts were estimated from[40]

$$\text{SLD} = \frac{dN_A \sum b_i}{M}, \tag{4}$$

where d is the mass density (g/cm^3) of the component, N_A is Avogadro's number, M is the molecular weight (g/mol) of the component, and Σb_i is the sum of the neutron scattering lengths of the atoms in the component. The calculated SLDs are listed in Table II.

III. RESULTS AND DISCUSSION

A. Dry state measurements

The initial dry thickness of the grafts in air was determined by ellipsometry and NR. The thicknesses from ellipsometry are listed in Table I and were used to calculate graft densities using Eq. (1).

Figure 1(a) shows the NR profiles for the dry layers (Table I). The reflectivity is multiplied by $(Q_z)^4$ to provide better resolution in comparing the data and the best fit in the high Q regime, because bare Si wafer follows the $(Q_z)^{-4}$

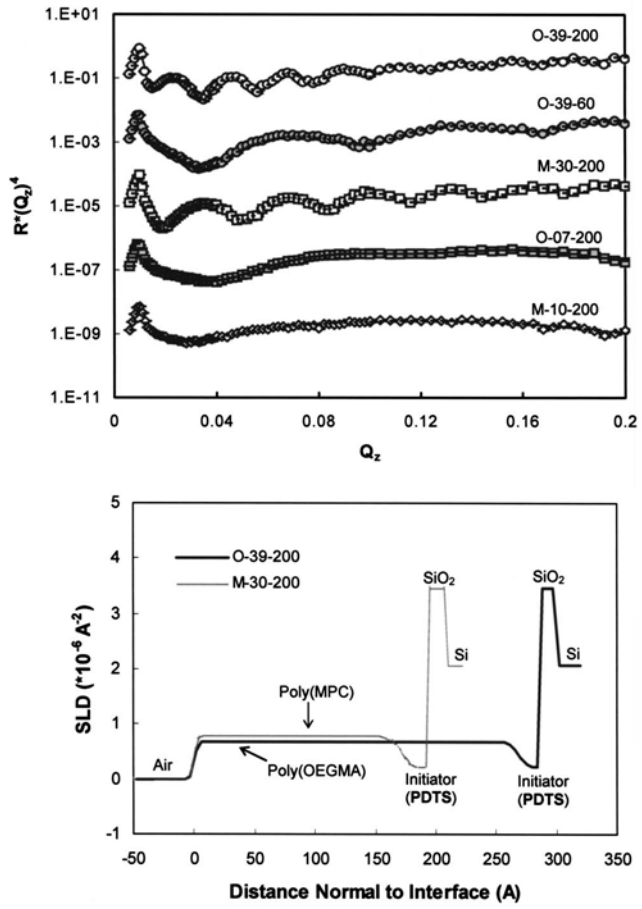

FIG. 1. (a) Neutron reflectivity profiles for the dry surfaces and their corresponding best fits (solid lines). The curves have been scaled by arbitrary factors for better viewing. (b) SLD profiles calculated using the best-fit data for the dry O-39-200 and M-30-200 surfaces.

decay. Data were fitted to a three-layer model using the PARRATT 32 software: SiO_2, the initiator layer, and the polymer layer. The SLDs of Si, SiO_2, the initiator layer, and air (ρ_{Si}, ρ_{SiO_2}, ρ_{init}, and ρ_{air}) were kept constant at the bulk values (Table II). All other parameters, i.e., layer thickness (d_{SiO_2}, d_{init}, and d_{poly}), interface roughness ($\sigma_{SiO_2/init}$, $\sigma_{init/poly}$, and $\sigma_{poly/air}$), and polymer layer SLD (ρ_{poly}), were allowed to vary to satisfy the minimum sum of squares criterion (χ^2). The best fits to the data (solid lines) are shown in Fig. 1(a). Kiessig fringes are clearly present in the reflectivity curves of the high graft density samples (O-39-200, O-39-60, and M-30-200), indicative of a uniformly thick sample, while the absence of Kiessig fringes in the low graft density samples, i.e., O-07-200 and M-10-200, is indicative of nonuniform thickness or rough surfaces. SLD profiles for the O-39-200 and M-30-200 surfaces are shown in Fig. 1(b).

The model parameters from the data fits for the dry samples are summarized in Table III. Thicknesses of 13–20 Å and 13–24 Å for the SiO_2 and initiator layers, respectively, are in good agreement with the values obtained by ellipsometry, viz., 17±2 and 20±3 Å.[34,41] The various polymer layer thicknesses are also in good agreement with the values obtained by ellipsometry (Table I). The roughness parameters show that the SiO_2 and initiator layers are relatively smooth: they are of uniform thickness with $\sigma_{SiO_2/init}$ from 0 to 5.9 Å and $\sigma_{init/poly}$ from 2.2 to 7.9 Å, values which compare well with the root-mean-square (rms) roughness of these two surfaces as measured by atomic force microscopy (AFM), viz., 1.9 and 4.5 Å.[41] For the polymer/air interface, however, the situation is somewhat different. At high graft density, the poly(OEGMA) (O-39-200 and O-39-60) and poly(MPC) (M-30-200) layers appear very smooth with values of $\sigma_{poly/air}$ from 0 to 2.7 Å. The low graft density M-10-200 surface is rougher with a value of 32.6 Å, whereas the O-07-200 surface is relatively smooth with a value of only 8.0 Å. In our previous work,[25] AFM images of high graft density surfaces showed smooth surfaces with typical rms roughness of ~3.0 Å. The M-10-200 surface showed peaks and valleys with rms roughness of 32.0 Å, a value much greater than that of the O-10-200 surface (6.0 Å).[25] The "roughness" data for the polymer layers, as determined by NR, are thus consistent with our previous AFM measurements.

B. Wet state measurements

One of the objectives of the present work was to investigate the conformational differences between poly(OEGMA) and poly(MPC) grafts in water, the medium most relevant to biomedical applications. Pure D_2O was chosen since it provides good neutron contrast for poly(OEGMA) and poly(MPC). Figure 2(a) shows the reflectivity profiles obtained in D_2O. Compared to Fig. 1(a), the Kiessig fringes in

TABLE III. Model parameters for grafted surfaces in dry state.

	O-39-200	O-39-60	M-30-200	O-07-200	M-10-200
d_{SiO_2} (Å)	13.6	14.0	13.5	20.8	18.0
$\sigma_{SiO_2/init}$ (Å)	0.0	1.7	0.0	5.6	5.9
d_{init} (Å)	17.0	13.0	23.7	19.5	18.1
$\sigma_{init/poly}$ (Å)	5.0	7.2	7.9	3.5	2.2
ρ_{poly} (10^{-6} Å^{-2})	0.68	0.74	0.81	0.59	0.67
d_{poly} (Å)	268.9	85.1	170.4	56.6	66.7
$\sigma_{poly/air}$ (Å)	2.0	0.0	2.7	8.0	32.6
χ^2	0.014	0.014	0.017	0.005	0.009

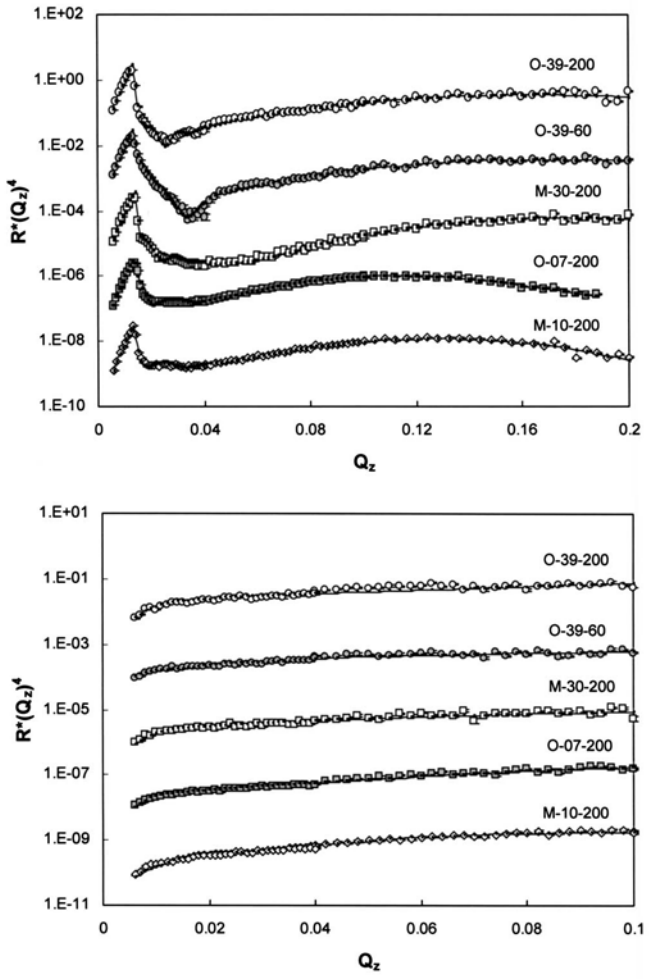

FIG. 2. Experimental neutron reflectivity curves for surfaces in (a) D_2O, (b) null-SLD water, and the corresponding best fits (solid lines) to the data. Intensities are offset by arbitrary factors to better distinguish the data.

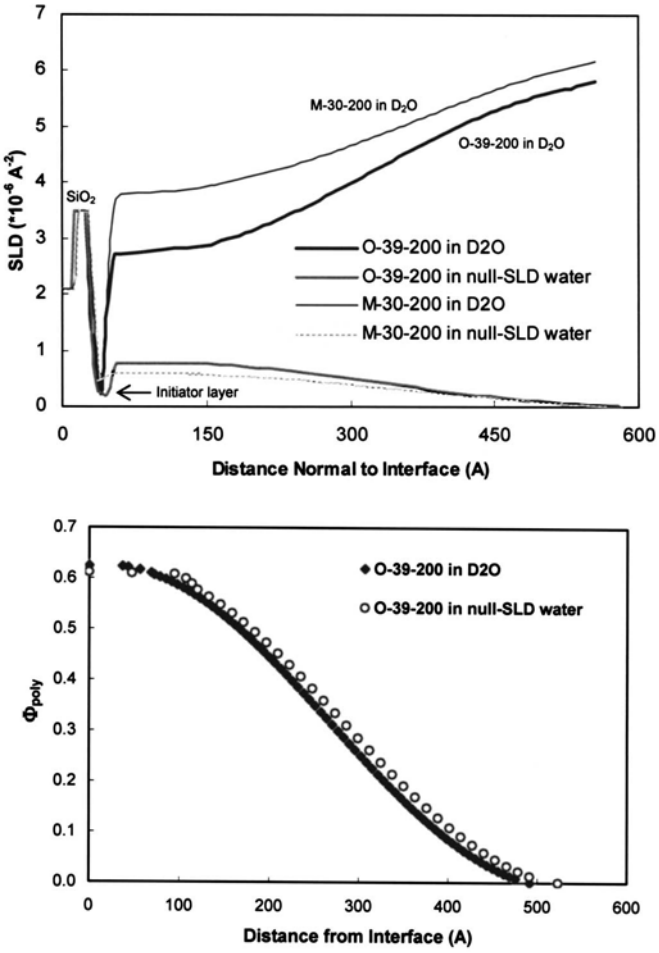

FIG. 3. (a) SLD profiles for O-39-200 and M-30-200 in D_2O and in null-SLD water. (b) Volume fraction profiles of O-39-200 in D_2O and in null-SLD water.

all cases are absent, indicating that at least one of the interfacial boundaries, presumably the polymer/water interface, was diffuse.

While the swelling behavior of monodisperse polymer brushes in solvents has been widely studied both theoretically[42–45] and experimentally,[27,28,39,46] little work has been done on polydisperse polymer grafts. For monodisperse polymer layers of moderate graft density and polydispersity (PDI) $\leqslant$1.1, the volume fraction of polymer versus distance ($\Phi_{poly}(z)$ vs z) follows Eq. (2).[28,40] Based on self-consistent mean field methods for polydisperse polymer chains,[47–50] $\Phi_{poly}(z)$ vs z profiles can assume parabolic, exponential, or linear decay forms depending on graft density, solvent quality, and the distribution of short and long chains. Recently, Yim *et al.*[29,51] reported parabolic decays for PNIPAM chains with PDI of 1.32 and 2.10 in water at 20 °C, a good solvent for PNIPAM. These PNIPAM chains were grafted from flat surfaces using surface-initiated ATRP.

Based on these considerations, the parabolic profile [Eq. (2)] was used to fit the wet state data in the present work. To reduce the number of fitting parameters, we adopted the values of d_{SiO_2}, d_{init}, $\sigma_{SiO_2/init}$, and $\sigma_{init/poly}$ from the best-fit results for the dry samples. Meantime, ρ_{Si}, ρ_{SiO_2}, and ρ_{init} were fixed at their bulk values. Figure 2(a) shows the best fits (solid lines) to the experimental reflectivity data.

To further validate the profiles of $\Phi_{poly}(z)$ vs z, NR measurements were also carried out using null scattering water as the solvent. Since null-SLD water has a net coherent SLD of $\sim$0, NR is sensitive only to the polymer layer structure. The null scattering water data were fitted using the parabolic decay model and are shown in Fig. 2(b). The SLD profiles of O-39-200 and M-30-200 in D_2O and in null-SLD water are shown in Fig. 3(a). A noteworthy feature of the SLD profiles is the dramatic jump between the initiator layer and the innermost polymer film, suggesting that the initiator layer acts as a hydrophobic barrier, impermeable to water.

From the SLD profiles presented in Fig. 3(a), the polymer volume fraction (Φ_{poly}) as a function of distance through the film can be calculated. Assuming that the volumes are additive, the SLD for a binary polymer/solvent system can be written as

$$\rho_{mix}(z) = \Phi_{poly}(z) \times \rho_{poly} + (1 - \Phi_{poly}(z)) \times \rho_{solvent}, \qquad (5)$$

where $\rho_{mix}(z)$ is the SLD of the polymer/solvent mixture at a distance z from the initiator layer, $\Phi_{poly}(z)$ is the polymer

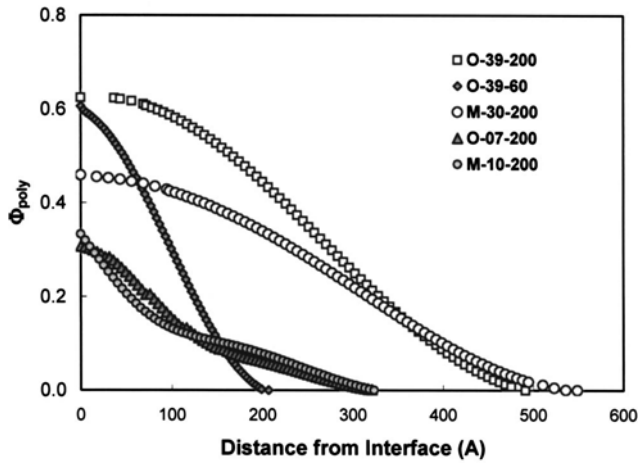

FIG. 4. Polymer volume fraction profiles for surfaces in D_2O.

volume fraction at distance z, and ρ_{poly} and $\rho_{solvent}$ are the SLDs of the pure polymer and the solvent (D_2O or null-SLD water), respectively. Figure 3(b) compares the volume fraction profiles for O-39-200 in D_2O and in null-SLD water calculated using the parabolic decay model. As can be seen, the two profiles are similar. The volume profiles in D_2O and null-SLD water for the other surfaces were also similar (data not shown), confirming that the volume fraction profiles of the polymer layers in water are valid and that the application of the parabolic decay model is appropriate. The polymer volume fraction profiles in D_2O for all the surfaces are shown in Fig. 4, while the parameters, $\Phi_{0,poly}$, h, and α, measured in D_2O and in null-SLD water, are listed in Table IV.

Solvent quality and graft density are two critical parameters in determining chain conformation and the values of $\Phi_{0,poly}$, h, and α. For the O-39-200 and O-39-60 surfaces, which have the same graft density of 0.39 chains/nm^2 but different chain lengths, the calculated $\Phi_{0,poly}$ for both surfaces in D_2O and null-SLD water was $\sim 0.63 \pm 0.01$. The values of α were also similar at $\sim 3.2 \pm 0.1$. For O-07-200 having a graft density of 0.07 chains/nm^2, $\Phi_{0,poly}$ was lower at 0.31 and α was higher at 6.07. These results suggest that the graft density directly affects $\Phi_{0,poly}$ and α, and that the higher the graft density, the greater the value of $\Phi_{0,poly}$ and the smaller the value of α. Similar effects have been observed by others. For example, Devaux *et al.*[52] reported $\Phi_{0,poly}=0.85$ for polystyrene (PS) brushes at a graft density of 1.1 chains/nm^2 in toluene, a good solvent for PS. Levicky *et al.*[53] reported $\alpha=2.5$ for dense PS brushes, and Kent *et al.*[39] found that the exponent α increased with decreasing graft density. As the graft density increases, it presumably becomes increasingly difficult for the solvent to penetrate the layers close to the substrate, leading to an incompletely swollen state, i.e., a high $\Phi_{0,poly}$ value. As shown in Table IV, the poly(OEGMA) thickness in the wet state decreased with decreasing chain length and graft density. For O-39-200, h is ~ 450 Å, close to the contour length of 500 Å, confirming that water is a good solvent for poly(OEGMA). Comparing M-30-200 and M-10-200, having the same chain length but

TABLE IV. Evaluation of NR data for grafted surfaces in D_2O and in null-SLD water.

	O-39-200		O-39-60		M-30-200		O-07-200		M-10-200	
	D_2O	Null-SLD water	D_2O	Null-SLD water	D_2O	Null-SLD water	D_2O	Null-SLD water	D_2O	Null-SLD water
$\Phi_{0,poly}$	0.62	0.63	0.61	0.64	0.47	0.49	0.31	0.31	0.35	0.35
h (Å)	431	452	141	149	467	479	211	211	265	265
α	3.19	3.16	3.29	3.29	2.15	2.17	6.07	6.07	8.83	8.83
ρ_{bulk} (10^{-6} Å^{-2})[a]	5.73	0.01	6.04	0.09	6.26	0.00	5.79	0.30	5.54	0.00
$\rho_{solvent}$ (10^{-6} Å^{-2})[b]	5.84	0.01	6.36	0.64	6.36	0.00	6.36	–0.27	6.36	0.00
$\rho_{polymer}$ (10^{-6} Å^{-2})[c]	0.89	1.25	1.01	1.54	0.85	1.23	1.40	1.40	0.46 8	0.46 8
$\sigma_{poly/solvent}$ (Å)	35	36	25	35	46	37	47	47	50	50
χ^2	0.67 6	0.35 0	0.20 4	0.20 3	0.15 6	0.03 9	0.22 3	0.01 7	0.63 6	0.11 8
$\bar{\Phi}_{poly}$	0.39	⋯	0.37	⋯	0.29	⋯	0.16	⋯	0.15	⋯
$N_{w,EO}$ or $N_{w,PC}$	4.9	⋯	5.4	⋯	30.4	⋯	16.5	⋯	73.6	⋯
Fg ads. (ng/cm^2)[d]	8±5		10±5		7±3		99±11		62±23	

[a]SLD of bulk solvent.
[b]SLD of solvent penetrated into polymer layer.
[c]SLD of polymer layer.
[d]Fibrinogen adsorption from 1 mg/mL TBS buffer (mean±SD, $n=6$) (Ref. 25).

different chain densities, it is again observed that $\Phi_{0,poly}$ and h decreased with decreasing graft density. The thickness of the wet M-30-200 layer is about 470 Å, implying that the poly(MPC) chains are highly extended in water.

For all samples examined, the interface between the polymer chains and water was very rough with $\sigma_{poly/solvent}$ ranging between 25 and 50 Å; there are two possible reasons: (1) the polydispersity of the chains and (2) local motions (fluctuations) of the chain ends, a phenomenon previously observed in monodisperse polymer systems.[28,43,44]

It is difficult to compare quantitatively the swelling behavior of poly(OEGMA) and poly(MPC) brushes in water because the polymer chains have different MW distributions and the graft densities of the two are not exactly the same. However, it appears that both poly(OEGMA) and poly(MPC) chains swell significantly in water, indicating strong interactions of these polymers with water. Since the differences in wet thickness at high σ (O-39-200, M-30-200) and low σ (O-07-200, M-10-200) are not significant, it appears that swelling behavior is similar.

C. Hydration effects

To further investigate the role of water in preventing protein adsorption to the tethered polymer layers, we calculated the average volume fractions of the polymer chains ($\bar{\Phi}_{poly}$) in the layers in contact with D_2O and null-SLD water (Table IV). The average numbers of water molecules per EO unit ($N_{w,EO}$) or per PC residue ($N_{w,PC}$) were then estimated based on the value of $\bar{\Phi}_{poly}$ and on the assumption that water does not interact significantly with the hydrophobic regions of the polymers. At high graft density (O-39-200 and O-39-60), $N_{w,EO}$ was found to be ~5, increasing to 16.5 at low graft density (O-07-200). For the poly(MPC) surfaces, $N_{w,PC}$ had a value of 30.4 at high density (M-30-200) and 73.6 at low density (M-10-200).

It should be noted that $N_{w,EO}$ and $N_{w,PC}$ are, respectively, the ratios of the total number of water molecules to the total number of EO and PC units in the polymer layers. The $N_{w,EO}$ and $N_{w,PC}$ values include water of hydration and bulk (free) water, in amounts that depend on the graft density. The water in the hydration layers is different from that in the bulk with respect to structure and properties. For example, it has been reported that, in general, the motion of water of hydration is much slower than that of free water.[54] In an attempt to correlate $N_{w,EO}$ and $N_{w,PC}$ to protein adsorption behavior, the values were compared with the number of water molecules in the hydration layers of the EO and PC residues, i.e., $N_{w',EO}$, and $N_{w',PC}$ respectively.

Both simulation and experimental data indicate that the number of water molecules in the hydration layer per EO unit of PEO, viz., $N_{w',EO}$, is ~2.5.[55,56] In the hydration layers surrounding PEO chains in dilute and semidilute solutions, water molecules may exist in a variety of states: hydrogen bonded to PEO (the first hydration layer), "indirectly" bonded as in the second hydration shell, and "quasifree." In concentrated PEO solutions, where the volume fraction of PEO is greater than 0.55, the hydration layer contains only water molecules hydrogen bonded to PEO.[55]

In this work, $N_{w,EO}$ was estimated to be of the order of 5 at high graft density, in good agreement with two recent NR experiments on PEO monolayers. Fick *et al.*[57] reported a volume fraction of 0.68 for water in a PEO-terminated self-assembled monolayer (SAM) of graft density 0.6 chains/nm^2 and PEO MW 2000 Da, resulting in $N_{w,EO}$ =5.4. Unsworth *et al.*[18] investigated the swelling behavior of a PEO layer chemisorbed on gold of graft density 0.99 chains/nm^2 and MW 750 Da. The water volume fraction in this system was found to be 0.61, corresponding to $N_{w,EO}$=3.8. Both of these PEO-SAMs were strongly protein resistant. The O-39-60 and O-39-200 layers reported in the present work have also been shown to be strongly protein resistant[25], with fibrinogen adsorption from a 1 mg/ml solution in buffer $\leqslant$10 ng/cm^2, a reduction of greater than 98% compared to the unmodified surfaces.

Unsworth *et al.*[18] also investigated a PEO layer of MW 750 Da and graft density 1.32 chains/nm^2. Protein adsorption on this surface was much greater than on the surface of graft density 0.99 chains/nm^2. The water volume fraction for the layer of higher graft density was found by NR to be 0.43 and $N_{w,EO}$ was 1.8, i.e., lower than the value of 2.5 for $N_{w',EO}$, indicating that there was no free water associated with the PEO chains.

For the O-07-200 layer, where the graft density of poly(OEGMA) was 0.07 chains/nm^2, $\bar{\Phi}_{poly}$ was found to have a value of 0.16, resulting in $N_{w,EO}$=16.5, suggesting an abundance of free water in the layer. On this surface, fibrinogen adsorption from a 1 mg/ml buffer solution was shown to be ~100 ng/cm^2, i.e., much greater than on the O-39-200 surface.[25] From the results of this work (and that of others as mentioned), it appears that the value of $N_{w,EO}$ is a good indicator of the state of water in the grafted PEO layers. For $N_{w,EO} > N_{w',EO}$ (~2.5), the hydration layer includes hydrogen bonded water and bulk water. The bulk water presumably increases the mobility of the PEO chains, thus contributing to protein resistance. For $N_{w,EO} \gg N_{w',EO}$, there is an abundance of bulk water in the layers. Protein adsorption is then greater, presumably due to the low coverage of PEO. For $N_{w,EO} < N_{w',EO}$, the water content is low, thus increasing the surface hydrophobicity; also the molecules in the hydration layer are presumably tightly bound to the PEO, thus reducing chain mobility. Both of these effects would tend to give surfaces of relatively high protein adsorption.[18]

Phosphatidyl choline monolayers and bilayers exhibit different phase behaviors depending on their packing density, water content, film pressure, and temperature.[58] The hydration number of a PC group ($N_{w',PC}$) varies from 4 in the solid (S) phase to 25 in the fluid (I) phase.[59] For poly(MPC) brushes in water, since their PC groups are present on the sidechains and are disordered compared to the PC groups in monolayers and bilayers of phospholipids, hydration behavior is much closer to that in the fluid phase. Based on predictions by Pandit and co-workers[60,61] a dipalmitoylphos-

phatidylcholine (DPPC) bilayer in the fluid phase has several hydration layers, e.g., water (N=6.6) which penetrates into the PC headgroup, water (N=6.0) in the primary hydration layer, and water (N=13.0) in the secondary hydration layer, giving $N_{w',PC}$ of 25.6. These values are in excellent agreement with calorimetric measurements by Ruocco and Shipley,[62] who found 23 water molecules/lipid residue in a DPPC bilayer, 12 of which were bound to the PC headgroup and 11 were trapped within the bilayer. For a monolayer of DPPC in the fluid phase,[59] it was found by NR that $N_{w',PC}$ is 22±2, which again compares favorably with $N_{w',PC}$ of 25.6 predicted by Pandit *et al.*[61] and of 23 by Ruocco and Shipley.[62] In another NR study of *n*-dodecyl phosphorylcholine ($C_{12}PC$) monolayers, Yaseen *et al.*[63] reported that $N_{w',PC}$ increased from ~15 to ~25 when the graft density decreased from 2.0 to 1.3 chains/nm^2. Moreover, a value of $N_{w',PC}$=28±5 was calculated from differential scanning calorimetry measurements based on the equilibrium water content in MPC block copolymers.[22] Based on the available evidence, it appears that the hydration behavior of a PC headgroup is similar in bilayers, monolayers, and MPC polymers.

For M-30-200, $N_{w,PC}$ was estimated to be 30.4, in agreement with the value of $N_{w',PC}$ reported for MPC block copolymers. For M-10-200, with graft density 0.10 chains/nm^2, $N_{w,PC}$ was found to be 73.6, suggesting an abundance of free water. For this surface, fibrinogen adsorption from a 1 mg/ml solution was 62±23 ng/cm^2, a value much greater than the 7±3 ng/cm^2 found for the M-30-200 surface.[25] Considering the estimated $N_{w,PC}$ values and the protein adsorption behavior, it is concluded that the poly(MPC)-grafted surfaces are protein resistant when $N_{w,PC} \sim N_{w',PC}$ (~25). For both graft types it thus appears that the water barrier effect is due mainly to the water of hydration.

IV. CONCLUSIONS

Investigation of the structures of grafted poly(OEGMA) and poly(MPC) layers on Si substrates (dry and wet state) using neutron reflectometry is reported. For the dry surfaces, estimates of thickness and roughness from neutron reflectometry data are consistent with ellipsometry and AFM data, respectively. In the wet state, the best-fit NR data for the surfaces in D_2O and null-SLD water are in agreement. The parabolic model, with a stretched exponent, adequately describes the polymer fraction in the layer as a function of distance from the surface for both high and low graft densities. From estimates of the average number of water molecules (N_w) per EO or PC moiety, it appears that the "water barrier" to protein adsorption is provided mainly by water in the bound state.

ACKNOWLEDGMENTS

One of the authors (W.F.) acknowledges M. S. Kent, Sandia National Laboratories, and Meng Chen, University of Oxford, for fruitful discussions and suggestions on the NR data analysis. Financial support of this work by the Natural Sciences and Engineering Research Council of Canada (NSERC), the Canadian Institutes of Health Research (CIHR), and the Canada Foundation for Innovation (CFI) is gratefully acknowledged. One of the authors (W.F.) is supported by an Ontario Graduate Scholarship for Science and Technology (OGSST).

[1]*Proteins at Interfaces II, Fundamentals and Applications*, ACS Symposium Series No. 602, edited by T. A. Horbett and J. L. Brash (American Chemical Society, Washington DC, 1995).
[2]D. G. Castner and B. D. Ratner, Surf. Sci. **500**, 28 (2002).
[3]J. L. Brash, J. Biomater. Sci., Polym. Ed. **11**, 1135 (2000).
[4]M. Tirrell, E. Kokkoli, and M. Biesalski, Surf. Sci. **500**, 61 (2002).
[5]B. Kasemo, Surf. Sci. **500**, 656 (2002).
[6]J. H. Lee and J. D. Andrade, Prog. Polym. Sci. **20**, 1043 (1995).
[7]M. Morra, J. Biomater. Sci., Polym. Ed. **11**, 547 (2000).
[8]A. L. Lewis, Colloids Surf., B **18**, 261 (2000).
[9]P. Vermette and L. Meagher, Colloids Surf., B **28**, 153 (2003).
[10]Y. Iwasaki and K. Ishihara, Anal. Bioanal. Chem. **381**, 534 (2005).
[11]P. Harder, M. Grunze, R. Dahint, G. M. Whitesides, and P. E. Laibinis, J. Phys. Chem. B **102**, 426 (1998).
[12]S. J. Sofia, V. Premnath, and E. W. Merrill, Macromolecules **31**, 5059 (1998).
[13]W. Norde and D. Gage, Langmuir **20**, 4162 (2004).
[14]G. L. Kenausis *et al.*, J. Phys. Chem. B **104**, 3298 (2000).
[15]L. D. Unsworth, H. Sheardown, and J. L. Brash, Langmuir **21**, 1036 (2005).
[16]D. J. Vanderah, L. La, J. Naff, V. Silin, and K. A. Rubinson, J. Am. Chem. Soc. **126**, 13639 (2004).
[17]J. Zheng, L. Y. Li, S. F. Chen, and S. Y. Jiang, Langmuir **20**, 8931 (2004).
[18]L. D. Unsworth, Z. Tun, H. Sheardown, and J. L. Brash, J. Colloid Interface Sci. **296**, 520 (2006).
[19]A. J. Pertsin and M. Grunze, Langmuir **16**, 8829 (2000).
[20]R. L. C. Wang, H. J. Kreuzer, and M. Grunze, J. Phys. Chem. **101**, 9767 (1997).
[21]R. Y. Wang, M. Himmelhaus, J. Fick, S. Herrwerth, W. Eck, and M. Grunze, J. Chem. Phys. **122**, 164702 (2005).
[22]K. Ishihara, H. Nomura, T. Mihara, K. Kurita, Y. Iwasake, and N. Nakabayashi, J. Biomed. Mater. Res. **39**, 323 (1998).
[23]H. Kitano, K. Sudo, K. Ichikawa, M. Ide, and K. Ishihara, J. Phys. Chem. B **104**, 11425 (2000).
[24]H. Kitano, M. Imai, T. Mori, M. Gemmei-Ide, Y. Yokoyama, and K. Ishihara, Langmuir **19**, 10260 (2003).
[25]W. Feng, S. P. Zhu, K. Ishihara, and J. L. Brash, BioInterphases **1**, 50 (2006).
[26]J. R. Lu, R. K. Thomas, and J. Penfold, Adv. Colloid Interface Sci. **84**, 43 (2000).
[27]M. S. Kent, L. T. Lee, B. J. Factor, F. Rondelez, and G. S. Smith, J. Chem. Phys. **103**, 2320 (1995).
[28]A. Karim, S. K. Satija, J. F. Douglas, J. F. Ankner, and L. Fetters, Phys. Rev. Lett. **73**, 3407 (1994).
[29]H. Yim, M. S. Kent, S. Mendez, G. P. Lopez, S. Satija, and Y. Seo, Macromolecules **39**, 3420 (2006).
[30]W. Feng, J. Brash, and S. P. Zhu, J. Polym. Sci., Part A: Polym. Chem. **42**, 2931 (2004).
[31]M. Husseman *et al.*, Macromolecules **32**, 1424 (1999).
[32]K. Matyjaszewski *et al.*, Macromolecules **32**, 8716 (1999).
[33]W. Feng, R. X. Chen, J. L. Brash, and S. P. Zhu, Macromol. Rapid Commun. **26**, 1383 (2005).
[34]W. Feng, J. L. Brash, and S. P. Zhu, Biomaterials **27**, 847 (2006).
[35]K. Jankova, X. Y. Chen, J. Kops, and W. Batsberg, Macromolecules **31**, 538 (1998).
[36]R. Iwata, P. Suk-In, V. P. Hoven, A. Takahara, K. Akiyoshi, and Y. Iwasaki, Biomacromolecules **5**, 2308 (2004).
[37]K. Yamamoto, Y. Miwa, H. Tanaka, M. Sakaguchi, and S. Shimada, J. Polym. Sci., Part A: Polym. Chem. **40**, 3350 (2002).
[38]T. A. Harroun, H. Fritzsche, M. J. Watson, K. G. Yager, O. M. Tanchak, C. J. Barrett, and J. Katsaras, Rev. Sci. Instrum. **76**, 065101 (2005).
[39]M. S. Kent, J. Majewski, G. S. Smith, L. T. Lee, and S. Satija, J. Chem. Phys. **108**, 5635 (1998).
[40]S. M. Sirard, R. R. Gupta, T. P. Russell, J. J. Watkins, P. F. Green, and K.

P. Johnston, Macromolecules **36**, 3365 (2003).
[41]W. Feng, S. P. Zhu, K. Ishihara, and J. L. Brash, Langmuir **21**, 5980 (2005).
[42]P. G. de Gennes, Macromolecules **13**, 1069 (1980).
[43]S. T. Milner, T. A. Witten, and M. E. Cates, Macromolecules **21**, 2610 (1998).
[44]E. B. Zhulina, O. V. Borisov, V. A. Pryamitsyn, and T. M. Birshtein, Macromolecules **24**, 140 (1991).
[45]S. T. Milner, Science **251**, 905 (1991).
[46]M. S. Kent, L. T. Lee, B. Farnoux, and F. Rondelez, Macromolecules **25**, 6240 (1992).
[47]M. S. Kent, B. J. Factor, S. Satija, P. Gallagher, and G. S. Smith, Macromolecules **29**, 2843 (1996).
[48]S. T. Milner, T. A. Witten, and M. E. Cates, Macromolecules **22**, 853 (1989).
[49]T. M. Birshtein, Y. V. Liatskaya, and E. B. Zhulina, Polymer **31**, 2185 (1990).
[50]G. Kritikos and A. F. Terzis, Polymer **46**, 8355 (2005).
[51]H. Yim, M. S. Kent, S. Mendez, S. S. Balamurugan, S. Balamurugan, G. P. Lopez, and S. Satija, Macromolecules **37**, 1994 (2004).
[52]C. Devaux, F. Cousin, E. Beyou, and J. P. Chapel, Macromolecules **38**, 4296 (2005).
[53]R. Levicky, N. Koneripalli, M. Tirrell, and S. Satija, Macromolecules **31**, 3731 (1998).
[54]N. J. Tao, S. M. Lindsay, and A. Rupprecht, Biopolymers **28**, 1019 (1989).
[55]E. E. Dormidontova, Macromolecules **35**, 987 (2002).
[56]G. Maisano, D. Majolino, P. Migliardo, S. Venuto, F. Aliotta, and S. Magazu, Mol. Phys. **78**, 421 (1993).
[57]J. Fick, R. Steitz, V. Leiner, S. Tokumitsu, M. Himmelhaus, and M. Grunze, Langmuir **20**, 3848 (2004).
[58]O. Albrecht, H. Gruler, and E. Sackmann, J. Phys. (Paris) **39**, 301 (1978).
[59]C. Naumann, T. Brumm, A. R. Rennie, J. Penfold, and T. M. Bayerl, Langmuir **11**, 3948 (1995).
[60]M. L. Berkowitz, D. L. Bostick, and S. Pandit, Chem. Rev. (Washington, D.C.) **106**, 1527 (2006).
[61]S. A. Pandit, D. Bostick, and M. L. Lerkowitz, J. Chem. Phys. **119**, 2199 (2003).
[62]M. J. Ruocco and G. G. Shipley, Biochim. Biophys. Acta **691**, 309 (1982).
[63]M. Yaseen, J. R. Lu, J. R. P. Webster, and J. Penfold, Langmuir **22**, 5825 (2006).